An Unequal Split Dual Three-Phase PMSM With Extended Torque-Speed Characteristics for Automotive Application

Sandeep V. Nair, *Student Member, IEEE*, Kunal Layek, and Kamalesh Hatua, *Member, IEEE*

***Abstract*—High gradability and wide operating speed range are critical requirements for heavy-duty trucks and off-road electric vehicles. The motor power rating used for such applications can be reduced by selecting a motor with a wide constant power speed range (CPSR). However, permanent magnet synchronous motors (PMSMs) with wide CPSR have limited overloading capability. The operating speed range, as well as the overloading capability, can be improved by increasing the base speed of a low CPSR three-phase PMSM, which results in overdesign. Further, using multigear transmission to achieve a wide operating speed range with a low power motor increases system weight, drivetrain complexity, and maintenance requirement. This article proposes a dual three-phase interior PMSM with an unequal split winding configuration and zero degree winding displacement (uneq0-PMSM) to extend the constant power region and improve the overloading capability without any machine overdesign. The winding split ratio for the proposed configuration is decided to achieve the desired torque-speed characteristic shape for a given requirement. Further, a transition algorithm for smooth changeover between two-winding operation during low-speed and one-winding operation for high-speed is also proposed. The proposed concepts are experimentally validated on a 1.5-kW uneq0-PMSM with 1:3 winding split ratio.**

***Index Terms*—Dual three-phase permanent magnet synchronous motors (DTP-PMSMs), electric vehicles (EVs), field weakening (FW), high-speed (HS) permanent magnet synchronous motors, winding changeover.**

I. Introduction

INTERIOR permanent magnet synchronous motors (IPMSMs) are commonly used for applications like electric vehicles (EVs), hybrid EVs, and aircraft. Heavy-duty electric trucks, off-road vehicles, and military vehicles have special requirements like hill climbing, obstacle negotiation, hard acceleration, cross-country sprint, and high-speed (HS) driving compared to passenger cars. IPMSMs can achieve this high initial traction requirement and peak power ratings with improved efficiency and power factor. However, the maximum operating speed of IPMSM drives are limited due to the limitation in the dc bus voltage, which is derived from a battery bank. Field weakening (FW) is commonly used to extend the operating region of IPMSM. The constant power speed range (CPSR) requirement for commercial passenger EVs are in the range of 4–7, whereas that of heavy-duty direct drive electric truck is up to 25 [1], [2]. This wide constant power requirement can be achieved by appropriate machine design together with FW. However, such motors with wide CPSR have limited overloading capability in the HS operation when the saliency ratio of the motor is low [3]. A high saliency ratio design results in increased manufacturing complexity and lower mechanical stability and, hence, is not suitable for heavy-duty EVs.

The overloading capability is high for PMSMs with low CPSR since the FW requirement is low. However, the low CPSR machines have a low operating speed range. The operating speed range of a low CPSR PMSM can be improved by re-rating [4]. The re-rated machine has fewer turns with more parallel paths than the original machine, which would increase the base speed of the machine, delaying the start of FW. However, this results in increase in the inverter switch current rating. DC–DC boost converters are also used in commercial EVs to increase the dc bus voltage, hence expanding the operating region. However, the magnetic components of the boost converter result in additional space and weight requirements, thus deteriorating the vehicle efficiency.

Multiphase PMSMs are gaining popularity in EV applications since they can expand power and speed range without any additional magnetic components. An open-end winding (OEW) PMSM with a floating capacitor at the auxiliary inverter is proposed in [5], [6] to achieve an extension of the operating speed range. However, since the auxiliary inverter supplies only reactive power, the drive operation is halted in the event of a fault in the main inverter or any one of the phase windings. Dual three-phase PMSM (DTP-PMSM) also provides increased power rating and operating speed range extension similar to OEW PMSM with improved fault tolerance [7]. FW concept with winding switching [8] is also used to extend the operating speed range. In this configuration, the effective stator turns are

Manuscript received November 18, 2021; revised February 19, 2022; accepted April 8, 2022. Date of publication April 21, 2022; date of current version June 24, 2022. This work was supported in part by the Ministry of Electronics and Information Technology (MeitY) under NAMPET Phase-3 program, Government of India, under Grant 25(12)/2019-ESDA and was developed jointly with Centre for Development of Advanced Computing (C-DAC), Thiruvananthapuram, India. Recommended for publication by Associate Editor K. Akatsu. *(Corresponding author: Sandeep V. Nair.)*

The authors are with the Power Electronics and Drives Group, Department of Electrical Engineering, Indian Institute of Technology Madras, Chennai 600036, India (e-mail: ee15d023@ee.iitm.ac.in; ee19d411@smail.iitm.ac.in; kamalesh@ee.iitm.ac.in).

Color versions of one or more figures in this article are available at https://doi.org/10.1109/TPEL.2022.3169335.

Digital Object Identifier 10.1109/TPEL.2022.3169335

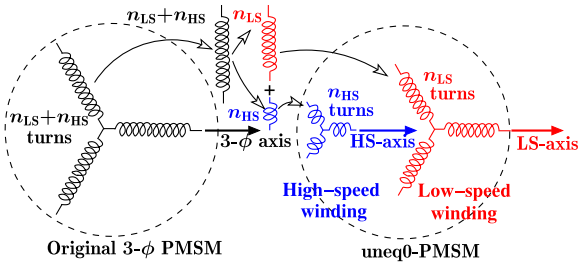

Fig. 1. uneq0-PMSM obtained from reconfiguration of three-phase PMSM.

reduced by changing the circuit configuration such that a part of the stator flux produced by the two winding sets connected in series opposes each other. Thus, the induced back electromotive force (EMF) of the winding reduces, increasing the base speed of the motor. However, the drive requires two isolated dc buses and results in additional stator copper loss since the rated stator current flows through the entire stator coils to produce a lower torque output during HS operation. It is to be noted that the operation in the HS region in all the above-discussed configurations are achieved using additional stator current, deteriorating its operating efficiency.

Winding changeover between star-delta, series–parallel [9], and their combinations [10] is also used to extend the operating speed range without additional stator current injection during HS operation. Further, motors with selection of appropriate section of winding using magnetic contactors [11] and matrix motors [12] are also used to achieve similar performance. However, these configurations necessitate a large number of ac contactors/bidirectional switches to achieve the desired operation. The matrix motor discussed in [13] requires isolated H-bridge converters for feeding each coil. A method of electronic winding change using a center tap in wye connected PMSM is proposed in [14] to extend the operating speed range with a minimal number of additional switches [two insulated gate bipolar transistors (IGBTs) and two diode bridge rectifiers]. However, in all these configurations, the winding changeover is performed when both the currently operating winding configuration and the target winding configuration are operated in their own below base-speed region, without utilizing the FW. Thus, the torque capability available with FW region is not fully utilized with these configurations. Therefore, a significant dip in the combined steady-state torque-speed characteristics with different winding interconnections is inevitable while using these winding changeover techniques.

In this article, an unequal split DTP-PMSM with 0° winding displacement (uneq0-PMSM) is proposed to achieve both extension of speed range as well as reduced FW requirement for improved overloading capacity and efficiency in the HS operating region. In uneq0-PMSM, the winding turns of the two three-phase winding sets are not equal and wound with 0° winding displacement between them. Hence, the uneq0-PMSM is the general case of the conventional DTP-PMSM (equal turns). The process of winding reconfiguration by which an uneq0-PMSM is obtained from a conventional three-phase PMSM is shown in Fig. 1 and the power circuit of the proposed drive is discussed in Section III (Fig. 9). In the proposed uneq0-PMSM, when the machine speed exceeds a specific speed, the three-phase winding set with higher number of turns [low-speed (LS) winding] is cut off using thyristor switches. As a result, the machine operates with only the three-phase winding set with lower number of turns (HS winding), achieving below base-speed control even in the HS operating region of the machine. The uneq0-PMSM has a different shape of torque-speed and power-speed characteristics compared to conventional three-phase PMSM, enabling the high efficiency operation in the HS region. The split ratio of winding turns can be chosen appropriately to suite the torque-speed characteristic for a given requirement. Thus, various torque-speed characteristics can be realized from a given IPMSM stator and rotor by only changing the winding split ratio using the proposed uneq0-PMSM configuration. As a result, the designer has an additional degree of freedom to achieve the torque-speed characteristics for a given application.

The major contributions of this article are as follows.

1) An uneq0-PMSM drive with thyristor switches for achieving desired torque-speed characteristics for heavy-duty transport trucks, off-road vehicles, and military trucks.
2) Extension of operating speed range with improved overloading capability and reduced d-axis current requirement during HS operation.
3) A smooth winding changeover method in FW region for complete utilization of available torque-speed characteristics.

The performance of the proposed concepts is validated on a 1.5-kW uneq0-PMSM drive with 1:3 winding split ratio.

II. Challenges in Machine Design for Medium-/Heavy-Duty Trucks and Military Vehicles

The typical medium-/heavy-duty trucks and military vehicles are characterized by very high tractive effort in the LS region for obstacle negotiation and hill climbing as shown in Fig. 2 [15]. Also, the tractive effort is low for HS operations like traffic cruising and HS highway driving. Since the speed of operation is low during high torque demand and vice versa, a motor power requirement of $18.6\,\mathrm{kW/ton}$ and CPSR of 24.7 can encompass all these continuous operating requirements as seen in Fig. 2. The load requirements like hard acceleration and emergency brake are only intermittent duty and, hence, can be met by overloading the $18.6\,\mathrm{kW/ton}$ machine for a short time. It is to be noted that the motor used for such an application should have a characteristic with a wide constant power operating region as shown in Fig. 2. However, if the constant power operating range of the motor used is limited, then it will result in an overdesign. The motors with a CPSR of 12.3, 8.2, 6.1, 4.9, and 4.1 are also able to satisfy the load requirement but requires a higher power rating of 37.3, 55.9, 74.6, 93.2, and 112 kW/ton, respectively, as seen from Fig. 2.

The torque-speed characteristics of the motor shown in Fig. 2 are ideal curves with a constant torque region followed by a constant power region (hyperbolic torque curve). However, the shape of torque-speed characteristics of an IPMSM is dependent on motor parameters and, hence, will deviate from the ideal

TABLE I
PARAMETERS OF VARIOUS THREE-PHASE IPMSM DESIGNS

Parameters	Spec-1	Spec-2	Spec-3
CPSR	24.7	5.87	4.8
ξ	2.6	2.6	2.6
$\Psi_{F(pu)}$	0.4803	0.5183	0.5444
$L_{d(pu)}$	0.4523	0.4067	0.3758
$L_{q(pu)}$	1.176	1.0574	0.9771

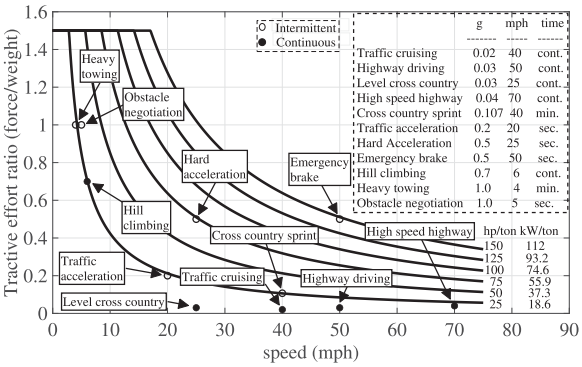

Fig. 2. Typical torque-speed characteristics requirement for a military truck [15].

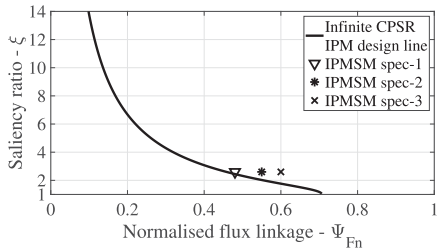

Fig. 3. Parameter plane for IPMSM design.

curve. The shape of torque-speed and power-speed characteristics of a surface-mount PMSM, IPMSM, and synchronous reluctance motor (SynRM) can be characterized using two independent variables: normalized flux linkage (Ψ_{Fn}) and saliency ratio (ξ) [3], [16]. Hence, the operating characteristics like maximum operating speed, CPSR, minimum magnet operating point in B-H curve, and power factor at base speed are decided by the location of the PMSM design parameters in the parameter plane ($\Psi_{\text{Fn}} - \xi$ plane).

Initially, three three-phase IPMSM design specifications (spec-1, spec-2, and spec-3) with different CPSR and same maximum torque (for satisfying high gradability) are considered in this article, which can be used for medium-/heavy-duty trucks and military vehicles. Hence, they should satisfy the load requirement in Fig. 2. The parameters of each design are given in Table I. The locations of the three three-phase IPMSM designs in the parameter plane are shown in Fig. 3. To ensure good mechanical robustness and ease of manufacturing, a saliency ratio of 2.6 is chosen for all designs. In this article, the base values for normalization are selected as the inverter voltage, rated current, and base speed of operation of three-phase IPMSM spec-1 with a CPSR of 24.7. Here, the IPMSM spec-1 has the same CPSR and, hence, is equivalent to the $18.6\,\text{kW/ton}$ machine given in Fig. 2.

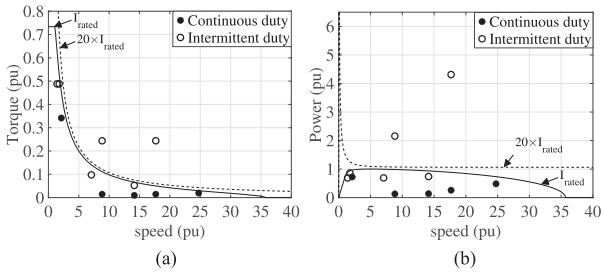

Fig. 4. Characteristics of three-phase IPMSM spec-1 with CPSR 24.7, $V_{\text{lim}} = 1$ p.u. (a) Torque-speed characteristics. (b) Power-speed characteristics.

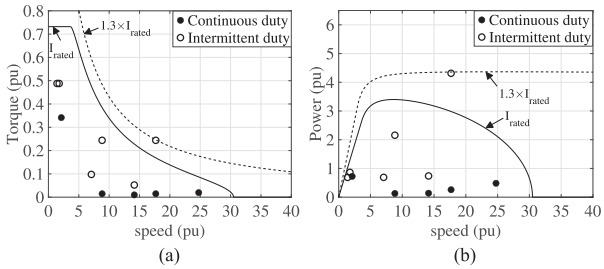

Fig. 5. Characteristics of three-phase IPMSM spec-2 with CPSR 5.87, $V_{\text{lim}} = 3.4$ p.u. (a) Torque-speed characteristics. (b) Power-speed characteristics.

Figs. 4–6 show the torque-speed and power-speed characteristics of three-phase IPMSM designs with spec-1, spec-2, and spec-3, respectively, superimposed with the typical operating points for military truck given in Fig. 2. The three-phase IPMSM spec-1 can satisfy all the continuous duty requirements without overrating, i.e., maximum space vector voltage of the inverter (V_{lim}) equals 1 p.u. as seen from Fig. 4. However, no significant improvement in developed torque at HS operation was observed even after overloading the machine with $20\times I_{\text{rated}}$ and, hence, was not able to satisfy the intermittent duty requirement. Thus, three-phase IPMSM spec-1 is not suitable for heavy-duty automotive requiring such high intermittent load capability during HS operation.

Increasing the power rating of three-phase IPMSM spec-1 (by increasing the dc bus voltage or by motor re-rating [4]) to satisfy the intermittent duty will not be a beneficial option compared to other designs; hence it is not considered in this article. Both three-phase IPMSM spec-2 and spec-3 can satisfy all the load requirements for the heavy-duty vehicle, as seen from Figs. 5 and 6. Here, an overcurrent of $1.3\times I_{\text{rated}}$ and $1.08\times I_{\text{rated}}$ is sufficient for three-phase IPMSM spec-2 and spec-3 to satisfy the intermittent duty requirements. However, the inverter dc bus voltage needs to be increased to 3.4 times and 4.47 times of spec-1 while using spec-2 and spec-3, respectively.

The proposed uneq0-PMSM can satisfy all the military truck requirements with the same dc bus voltage as three-phase IPMSM spec-1, as shown in Figs. 7 and 8. Fig. 7 shows the torque-speed and power-speed characteristics of uneq0-PMSM obtained by reconfiguring the windings of spec-2 with a 1:12 winding split ratio. Whereas, Fig. 8 shows the characteristics of uneq0-PMSM obtained from spec-3 with a 1:13 winding split ratio. Here, the winding split ratios are decided to exactly match the load requirement with minimal overdesign. An overcurrent of $6\times I_{\text{rated}}$ is required for both uneq0-PMSM with spec-2

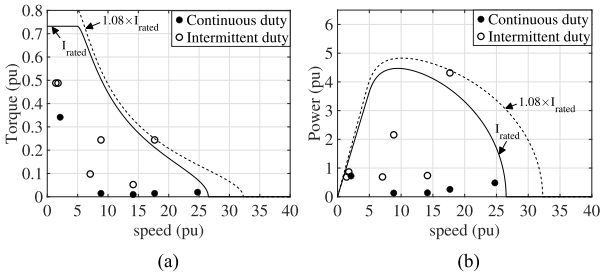

Fig. 6. Characteristics of three-phase IPMSM spec-3 with CPSR 4.8, $V_{\text{lim}} = 4.47$ p.u. (a) Torque-speed characteristics. (b) Power-speed characteristics.

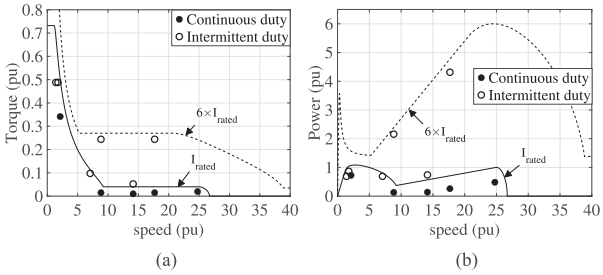

Fig. 7. Characteristics of uneq0-PMSM using reconfigured spec-2 with CPSR 5.87, $V_{\text{lim}} = 1$ p.u. (a) Torque-speed characteristics. (b) Power-speed characteristics.

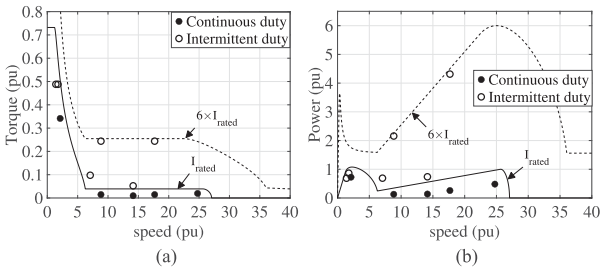

Fig. 8. Characteristics of uneq0-PMSM using reconfigured spec-3 with CPSR 4.8, $V_{\text{lim}} = 1$ p.u. (a) Torque-speed characteristics. (b) Power-speed characteristics.

TABLE II
COMPARISON OF VARIOUS IPMSM DESIGNS WITH THREE-PHASE AND UNEQ0-PMSM CONFIGURATIONS FOR MILITARY TRUCK

Parameters	Spec-1	Spec-2		Spec-3	
	3-ϕ PMSM	3-ϕ PMSM	uneq0-PMSM	3-ϕ PMSM	uneq0-PMSM
Split ratio			1:12		1:13
Requirement satisfied	No	Yes	Yes	Yes	Yes
DC bus voltage (pu)	1	3.4	1	4.47	1
No. 3-phase inverters	1	1	2	1	2
Over current req. ($\times I_{\text{rated}}$)	-	1.3	6	1.08	6
Peak power with I_{rated} (pu)	1	3.4	1.08	4.47	1.08
Base speed with T_{rated} (pu)	1	3.6	1.15	4.93	1.19
Max. operating speed (pu)	35.7	30.49	26.7	26.52	27.05

and spec-3 to encompass the intermittent operating points. A comparison of the performance of various IPMSM designs in three-phase and uneq0-PMSM configurations for military truck is comprehended in Table II. The advantages of the proposed uneq0-PMSM compared to other topologies are highlighted in gray. The detailed power structure and control system of the proposed uneq0-PMSM drive with programmable torque-speed capability [17] is discussed in the following section.

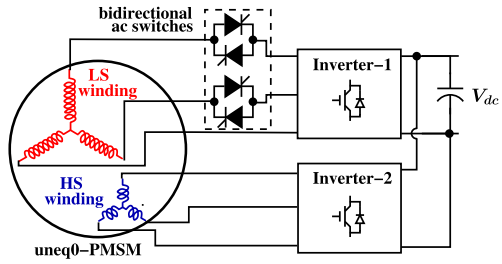

Fig. 9. Power circuit of the proposed uneq0-PMSM.

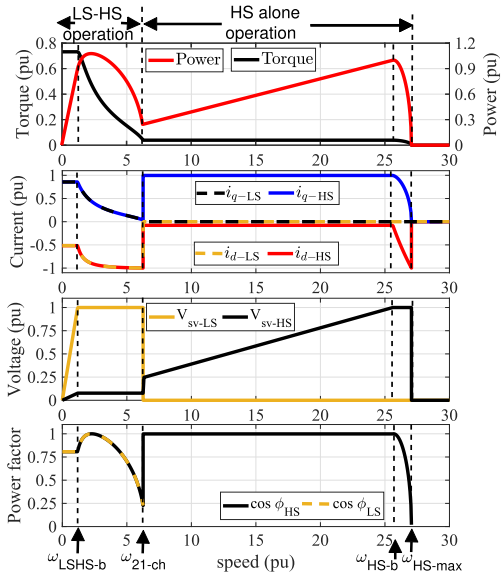

Fig. 10. Operation of the proposed uneq0-PMSM (spec-3 with 1:13 split).

III. VARIABLE TORQUE-SPEED CHARACTERISTICS USING THE PROPOSED DUAL THREE-PHASE PMSM WITH UNEQUAL SPLIT WINDING

The power circuit diagram of the proposed dual three-phase PMSM with unequal turns ratio (uneq0-PMSM) is shown in Fig. 9. The uneq0-PMSM is derived by reconfiguring only the stator winding of a conventional three-phase PMSM. The winding turns of the three-phase stator is split serially in an unequal proportion to derive two three-phase winding sets. The winding with a higher number of turns is denoted as the LS winding, and the winding with a lower number of turns is represented as the HS winding. The wire gauges and insulation levels of both LS and HS windings are equal to that of the original three-phase PMSM. The two winding sets have isolated neutrals and are fed from two similar rated inverters with a common dc bus, as shown in Fig. 9. Here, the two three-phase winding sets have 0° spacial displacement with respect to each other. Two back-to-back connected thyristors are also connected between the inverter-1 and LS winding to disconnect that winding during HS operation.

The operation of the proposed uneq0-PMSM is demonstrated in Fig. 10, showing the variation of torque, power, $d-q$ currents, and power factor of both LS and HS windings with the motor speed. The optimal values of reference d-axis and q-axis currents

are obtained from a predefined lookup table (LUT). The LUT is derived by solving the machine model in MATLAB such that the maximum torque output is generated with a minimal current while satisfying the voltage and current limits of the drive.

Both LS and HS windings are operated together in the below base-speed region during LS operation to extract maximum output torque from the machine. Since two three-phase windings are aligned to each other, the maximum output torque with minimum current is achieved when the current space vectors of both windings are also aligned. Hence, equal d-axis ($i_{d\text{-LS}}$=$i_{d\text{-HS}}$) and q-axis currents ($i_{q\text{-LS}} = i_{q\text{-HS}}$) are injected in both windings to achieve maximum torque per ampere (MTPA) operation, as seen from Fig. 10. As the operating speed increases and crosses the base speed of combined LS-HS winding operation ($\omega_{\text{LSHS-b}}$), FW is initiated in both windings by injecting more negative d-axis current to maintain the terminal voltage of LS winding at the maximum limit. The maximum voltage limit is set as the output voltage at the limit of linear modulation using space vector pulsewidth modulation (SVPWM). However, beyond a specific speed ($\omega_{\text{LSHS-max}}$), the LS winding cannot be operated since it exceeds the current or voltage limit even with FW. Hence, the pulses to the back-to-back connected thyristor switches are disabled to isolate the LS winding from inverter-1 at a prespecified speed ($\omega_{21\text{-ch}}$). Consequently, the power circuit changes to a conventional three-phase configuration where only the HS winding is operated from inverter-2. Thus, the current in LS winding reduces to zero as observed in Fig. 10. In the proposed uneq0-PMSM, the winding split ratio of the machine is decided such that the base speed of HS winding operated alone ($\omega_{\text{HS-b}}$) is greater than $\omega_{\text{LSHS-max}}$. Hence, the HS winding is operated in the below base-speed region after transition even though the machine is operating in the medium-speed/HS region. This below base-speed operation even during medium speed/HS using the proposed uneq0-PMSM improves its overload capability and reduces the additional d-axis current requirement compared to conventional three-phase PMSM with high CPSR to satisfy the similar load torque requirement. As the speed increases further, the FW is used in the HS winding by injecting more $-i_{d\text{-HS}}$ to extract its full torque capability and to achieve a wide operating speed range, as seen from Fig. 10. The maximum operating speed with HS winding operated alone is denoted as $\omega_{\text{HS-max}}$. The power factor of the machine is near unity in both LS (combined LS-HS winding operation) and medium-speed region (HS winding alone operation), whenever the operation is with below base-speed control. Hence, the machine efficiency and overload capability are improved compared to conventional three-phase or DTP-PMSM with high CPSR, whose major operating region is in FW.

A. *Effect of Variation of Split Ratio on uneq0-PMSM Characteristics*

Different shapes of torque-speed and power-speed characteristics are obtained by varying the winding split ratio of uneq0-PMSM. Fig. 11 shows various characteristics when three-phase IPMSM spec-3 is connected as three-phase, DTP, and uneq0-PMSM with different winding split ratios. The total number

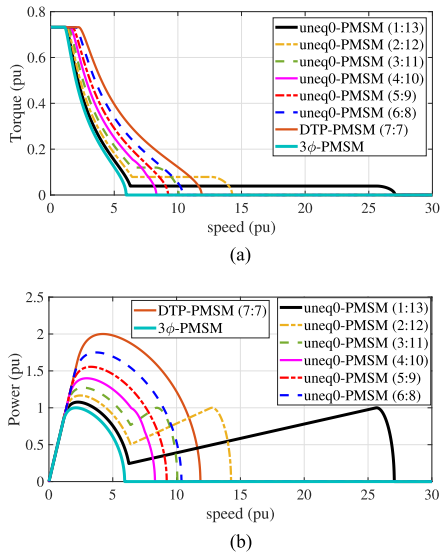

Fig. 11. Variation of power-speed and torque-speed characteristics with split ratio in uneq0-PMSM (spec-3). (a) Torque-speed characteristics. (b) Power-speed characteristics.

of turns per phase of three-phase PMSM spec-3 is assumed to be 14. Here, DTP-PMSM forms a subset of uneq0-PMSM when the winding split ratio is 7:7 (equal split). The feasible winding split ratios for uneq0-PMSM are 1:13, 2:12, 3:11, 4:10, 5:9, and 6:8 since there are 14 turns per phase. The resulting uneq0-PMSM with 6:8, 5:9, and 4:10 split ratios has a reduced operating area in the torque-speed and power-speed characteristics compared to DTP-PMSM. However, with a 3:11 split ratio, the shape of torque-speed characteristics starts to deviate from conventional three-phase PMSM. It consists of an LS region where two windings are operated and an HS region with one-winding operation. During the one-winding operation (HS winding alone), the machine is operated below the base-speed region by disconnecting the LS winding from the inverter, extending its operating speed range compared to two-winding configuration. This extended operation with one winding gets more prominent with the winding split ratios of 2:12 and 1:13. The resulting shapes of torque-speed characteristics with such extreme split ratios fit the heavy-duty automotive requirements discussed in Section II. The control of uneq0-PMSM with two-winding operation is discussed as follows.

B. *Control of the Proposed uneq0-PMSM*

The control system for the proposed uneq0-PMSM is shown in Fig. 12. Since the target application of the proposed drive is EVs, the drive is controlled using sensored vector control in current control with proportional–integral controllers. An LUT is used to generate the optimal reference currents for both windings to achieve MTPA operation. Since the reference currents for FW is also programmed in the LUT, no additional controller or algorithm is used to implement FW. During two-winding operation (combined LS-HS winding), the same reference currents from "i_d–i_q LS-HS LUT" are given to $d-q$ current controllers of LS and HS windings by selecting the switch position "0" in Fig. 12.

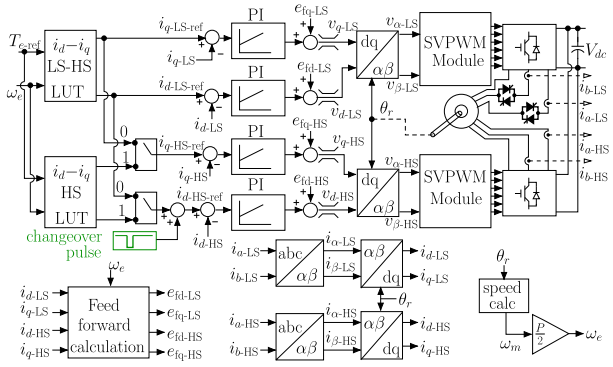

Fig. 12. Control system of the proposed uneq0-PMSM with sensored vector control.

During one-winding operation (HS winding alone), the switch position is changed to "1" to choose the reference currents from "i_d-i_q HS LUT."

"i_d-i_q LS-HS LUT" is implemented to obtain maximum output torque with minimal stator current and satisfy the voltage and current limit constraints during two-winding operation. Since the LS winding has a higher number of turns than the HS winding, the terminal voltage of HS winding is inherently controlled within limits when the terminal voltage of LS winding is limited. Hence, only the terminal voltage of LS winding needs to be restricted within the maximum inverter capability by FW as motor speed increases. The constraints used to derive "i_d-i_q LS-HS LUT" are as follows:

1) $V_{\text{sv-LS}} \le V_{\text{lim}}$; $I_{\text{ph}} \le I_{\text{lim}}$;
2) maximize developed torque (T_e).

$$T_e = \frac{2}{3}\frac{P}{2}(d_1 i_{q\text{-LS}} + d_2 i_{q\text{-HS}}) \times \left(\frac{3}{2}\Psi_F + (L_{md} - L_{mq})(d_1 i_{d\text{-LS}} + d_2 i_{d\text{-HS}})\right) \quad (1)$$

$$= \frac{2}{3}\frac{P}{2}\left(\frac{3}{2}\Psi_F i_q + (L_{md} - L_{mq}) i_d i_q\right). \quad (2)$$

Here, $V_{\text{sv-LS}}$ is the space vector voltage of LS winding, I_{ph} is the phase current, I_{lim} is the maximum current rating of the machine, i_q is the q-axis current, and i_d is the d-axis current. d_1 and d_2 are the winding split ratios with respect to total number of turns, where $d_1 = \frac{n_{\text{LS}}}{n_{\text{LS}}+n_{\text{HS}}}$; $d_2 = \frac{n_{\text{HS}}}{n_{\text{LS}}+n_{\text{HS}}}$. Further, $I_{\text{ph}} = I_{\text{ph-LS}} = I_{\text{ph-HS}}$, $i_q = i_{q\text{-LS}} = i_{q\text{-HS}}$, $i_d = i_{d\text{-LS}} = i_{d\text{-HS}}$. Ψ_F, L_{md}, and L_{mq} are permanent magnet flux, d-axis magnetizing inductance, and q-axis magnetizing inductance, respectively, of the original three-phase PMSM. Since during two-winding operation, rated current flows through the entire winding, the uneq0-PMSM has the same torque-speed characteristics shape and maximum torque as the original three-phase PMSM.

"i_d-i_q HS LUT" is derived considering the HS winding operation alone. Let n_{LS} and n_{HS} be the number of turns per phase in LS and HS winding, respectively. Since only HS winding is operated, the machine equations are the same as that of a three-phase PMSM with n_{HS} turns per phase. Since the rated current flows only through n_{HS} turns, the shape of torque-speed characteristics is different from the original three-phase PMSM from which it is derived, with $T_{e\text{-HS}}$ as the maximum torque rating. The constraints for "i_d-i_q HS LUT" implementation are as follows:

1) $V_{\text{sv-HS}} \le V_{\text{lim}}$; $I_{\text{ph-HS}} \le I_{\text{lim}}$;
2) maximize developed torque ($T_{e\text{-HS}}$)

$$T_{e\text{-HS}} = \frac{2}{3}\frac{P}{2}\left(\frac{3}{2}\Psi_{F\text{-HS}} i_{q\text{-HS}} + (L_{md\text{-HS}} - L_{mq\text{-HS}}) i_{d\text{-HS}} i_{q\text{-HS}}\right) \quad (3)$$

where $\Psi_{F\text{-HS}} = d_2\Psi_F$; $L_{md\text{-HS}} = d_2^2 L_{md}$; and $L_{mq\text{-HS}} = d_2^2 L_{mq}$. Here, $\Psi_{F\text{-HS}}$, $L_{md\text{-HS}}$, and $L_{mq\text{-HS}}$ are permanent magnet flux, d-axis magnetizing inductance, and q-axis magnetizing inductance, respectively, of the uneq0-PMSM with HS winding operated alone.

The voltage equations of LS and HS windings of the proposed uneq0-PMSM and the uneq0-PMSM parameter notations are given in Appendix. The coupling voltages of the LS and HS windings in the synchronous $d-q$ frame are given by

$$e_{\text{fd-LS}} = -\omega_e(L_{ls\text{-LS}} + L_{mq\text{-LS}}) i_{q\text{-LS}} - \omega_e(L'_{lm} + L_{mq\text{-LSHS}}) i_{q\text{-HS}} \quad (4)$$

$$e_{\text{fq-LS}} = \omega_e(L_{ls\text{-LS}} + L_{md\text{-LS}}) i_{d\text{-LS}} + \omega_e(L'_{lm} + L_{md\text{-LSHS}}) i_{d\text{-HS}} + \frac{3}{2}\omega_e \Psi_{F\text{-LS}} \quad (5)$$

$$e_{\text{fd-HS}} = -\omega_e(L_{ls\text{-HS}} + L_{mq\text{-HS}}) i_{q\text{-HS}} - \omega_e(L'_{lm} + L_{mq\text{-LSHS}}) i_{q\text{-LS}} \quad (6)$$

$$e_{\text{fq-HS}} = \omega_e(L_{ls\text{-HS}} + L_{md\text{-HS}}) i_{d\text{-HS}} + \omega_e(L'_{lm} + L_{md\text{-LSHS}}) i_{d\text{-LS}} + \frac{3}{2}\omega_e \Psi_{F\text{-HS}}. \quad (7)$$

The coupling voltages are fed forward to the current controller output as shown in Fig. 12 to achieve decoupled current control. SVPWM is used to generate gate pulses from the reference voltages in $\alpha-\beta$ stationary reference frame to control the uneq0-PMSM drive. A transition algorithm is used to obtain a smooth changeover from two-winding operation to one-winding when the speed increases and vice versa when speed decreases.

C. Transition From Two-Winding to One-Winding Operation and Vice Versa

A transition from two-winding operation to one-winding is performed at a predefined speed ($\omega_{12\text{-ch}}$) when the generated torque of the machine with HS winding operated alone exceeds the generated torque with combined LS-HS winding operation. During one-winding operation, LS winding should be isolated from inverter-1 using thyristor switches. However, a direct switch-OFF of LS winding results in an overcurrent since both LS and HS windings operate in the FW region at $\omega_{12\text{-ch}}$. This condition is similar to a control interruption during FW operation of a three-phase PMSM, resulting in uncontrolled regeneration. Therefore, conventionally, the winding transition is performed in the below base-speed region of operation itself in the traditional winding changeover methods [9]–[11], [14] and, therefore, is not able to fully utilize the machine torque capability available with FW.

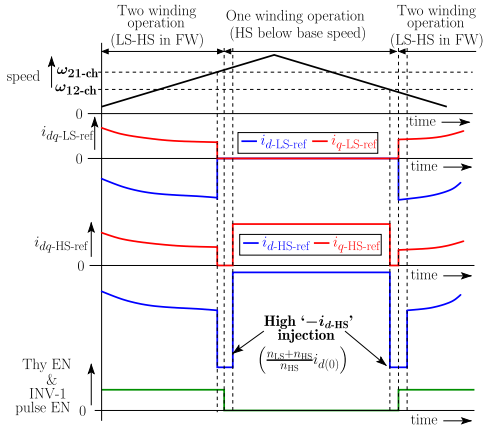

Fig. 13. Transition from two-winding operation to one-winding and vice versa.

The proposed uneq0-PMSM consists of two windings fed from two independent inverters. Hence, in the proposed transition algorithm, an additional d-axis current is injected from the HS winding to compensate for the decrease in the current contribution from LS winding during the transition. The additional d-axis current that needs to be injected from HS winding is $-\frac{n_{LS}}{n_{HS}} i_{d(0)}$, where $i_{d(0)}$ denotes the d-axis current at the changeover speed with zero torque output when both windings were operating. Thus, the uneq0-PMSM maintains FW even during the transition interval to achieve a smooth LS winding turn-OFF.

The transition process is explained using various reference currents, inverter-1 pulse enable (INV-1 pulse EN) and thyristor enable (Thy EN), as shown in Fig. 13. The transition algorithm is initiated whenever the operating speed crosses the predefined changeover speed for two- to one-winding ($\omega_{21\text{-ch}}$). The $d-q$ reference currents of LS winding and q-axis current reference of HS winding are changed to zero at the transition instant, as seen from Fig. 13. To maintain the FW operation, the d-axis current reference of HS winding is changed to $-\frac{n_{LS}+n_{HS}}{n_{HS}} i_{d(0)}$. Here, $-\frac{n_{LS}}{n_{HS}} i_{d(0)}$ component represents the additional current flowing through HS winding to maintain FW and to compensate for the loss of LS winding. Once the actual machine currents attain near steady-state, the thyristor switches and inverter-1 pulses are turned OFF to isolate LS winding from inverter-1. The changeover process is completed by selecting the current reference for HS winding from "$i_d - i_q$ HS LUT" to continue the machine operation in below base-speed with HS winding operated alone. It is to be noted that the generated torque becomes zero for a short duration during the winding transition. However, the performance of the considered applications including medium-/heavy-duty trucks, military vehicles, and even passenger cars are not affected by the short time torque dip due to their large inertia. The duration of control transition depends on the current controller bandwidth.

A flow diagram of the proposed transition process from two-winding to one-winding and vice versa is provided in Fig. 14. It is to be noted that, during two- to one-winding changeover, a delay is provided between disabling inverter pulses as well as thyristor pulses and change of HS winding current references. Similarly,

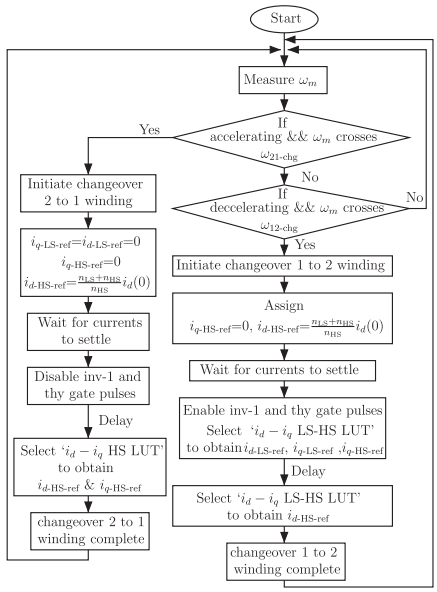

Fig. 14. Flow diagram of winding transition from two-winding operation to one-winding and vice versa for the proposed uneq0-PMSM.

during one- to two-winding changeover, a delay is introduced between enabling of inverter pulses as well as thyristor pulses and change of HS winding current references. This ensures that the high negative current reference of HS winding is not removed before the transition process is completed.

The uneq0-PMSM with parameters given in Table IV is simulated in MATLAB/Simulink to evaluate the proposed control as shown in Fig. 15. The motor speed is ramped up from 100 to 2570 r/min and back to 100 r/min by operating the load induction motor in speed control and uneq0-PMSM in torque control (which is set to achieve maximum generated torque at a given speed). The FW of LS winding is maintained during the winding transition from two- to one-winding and vice versa by injecting a high negative d-axis current in the HS winding as shown in the inset of Fig. 15(c). A smooth turn-ON and turn-OFF of LS winding with minimum current overshoot is observed in the LS winding phase current waveform given in the inset of Fig. 15(e).

IV. Comparison of Proposed uneq0-PMSM With Existing Winding Changeover Techniques

The general torque-speed and power-speed characteristics of all winding changeover techniques can be represented as shown in Fig. 16. Here, T_{max1} and T_{max2} represent the maximum generated torque with the highest equivalent turns configuration and the lowest equivalent turns configuration, respectively. Also, ω_{b1} and ω_{b2} represent the corresponding base speeds of torque characteristics corresponding to T_{max1} and T_{max2}, respectively. Fig. 16 represents the torque-speed and power-speed characteristics considering the operation of high equivalent turns winding in below base-speed region. Fig. 17 represents the corresponding characteristics with FW during the operation of high equivalent turns. It is observed that a significant power dip occurs in the power-speed characteristics in the vicinity of transition from

TABLE III
COMPARISON OF PROPOSED UNEQ0-PMSM AND EXISTING WINDING CHANGEOVER METHODS

Winding changeover topology	Ref	No. IGBT	Inv. type (no.)	No. bi-dir switches	Total eq. sw	T_{max} ratio	ω_b ratio	$P_{cu\text{-}2}$	FW1 present	Winding OC fault tolerance	Circ. current	Var. $T-\omega$ chara	rev. trans. to high eq.
Star-delta	[19], [20]	6	3-leg (1)	6	18	1:0.58	1:1.73	0.58	No	Yes	Yes	No	-
	[21]	14	3-leg (2)	0	14								
Series-parallel	[9], [22]	6	3-leg (1)	9	24	1:0.5	1:2	0.25	No	No	No	No	-
Tapped	[11]	6	3-leg (1)	6	18	1:x	1:$\frac{1}{x}$	x	No	No	No	Yes	-
	[14]	8		Nil	-								
	[23]	12		Nil	12				ND				
Combined tapped and star-delta	[10], [24]	6	3-leg (1)	12	30	1:0.58:x:0.58x	1:1.73:$\frac{1}{x}$:$\frac{1.73}{x}$	0.58	No	Yes	Yes	Yes	-
Five-phase	[25]	10	5-leg (1)	15	40	1:0.851:0.525	1:1.17:1.9	0.851	Yes	Yes	Yes	No	No
Series-end winding	[26]	8	4-leg (1)	4	16	1:0.58	1:2	0.58	ND	Yes	No	No	-
OEW PMSM	[8]	12	3-leg (2)	2	16	1:0.58	1:1.73	1	Yes	Yes	No	-	ND
	[18]												Yes
Cumulative-diff mode	[27]	6	3-leg (1)	6	18	1:0.268	1:3.73	1	No	No	No	-	-
	[28]			12	30	1:0.58:0.27:0.16	1:1.73:3.73:6.46				Yes		
uneq0-PMSM		12	3-leg (2)	2	16	1:x	1:$\frac{1}{x}$	x	Yes	Yes	No	Yes	Yes

ND : Not demonstrated
P_{cu2} : Copper loss during low equivalent turns operation in p.u.
Var. $T-\omega$ chara. : Ability to change the ratio of maximum torque and base speed of two windings by varying the ratio winding turns during design stage
FW1 present : Ability to operate the high equivalent turns in field weakening region before changeover to low equivalent turns
Rev. trans. to high eq. : Ability for reverse transition from "low eq. turns winding" to "high eq. turns winding in FW region" without uncontrolled regeneration
Circ. current : Circulating current during delta connected operation due to triplen harmonic in back EMF.

TABLE IV
PARAMETERS OF EXPERIMENTAL UNEQ0-PMSM PROTOTYPE

Parameter	Value	Parameter	Value	Parameter	Value
P_{rated}	1.5 kW	$R_{s\text{-LS}}$	4.874 Ω	$R_{s\text{-HS}}$	1.625 Ω
V_{dc}	300 V	$\Psi_{F\text{-LS}}$	0.8684 Wb	$\Psi_{F\text{-HS}}$	0.2894 Wb
Poles	4	$L_{sd\text{-LS-noload}}$	54 mH	$L_{sd\text{-HS-noload}}$	6 mH
I_{rated}	6 A	$L_{sq\text{-LS-noload}}$	101.54 mH	$L_{sq\text{-HS-noload}}$	11.284 mH
$\omega_{\text{HS-max}}$	2570 rpm	$L_{sd\text{-LS-load}}$	26.1 mH	$L_{sd\text{-HS-load}}$	2.9 mH
T_{rated}	32 Nm	$L_{sq\text{-LS-load}}$	94.5 mH	$L_{sq\text{-HS-load}}$	10.496 mH

the highest equivalent turns to lower equivalent turns operation when FW is not utilized during high equivalent turns operation, as shown in Fig. 16(b). This power dip could be reduced to a large extent if the FW of high equivalent turns was possible, as seen from Fig. 17(b).

In most of the conventional winding changeover methods, the high equivalent turns winding is operated in the below base-speed region, and the FW operation is not utilized. It is to be noted that some of the methods have demonstrated the FW operation of high equivalent turns configuration. In such methods, a transition from high equivalent turns to low equivalent turns is used to demonstrate the FW operation of high equivalent turns. However, a reverse transition from low equivalent turns to high equivalent turns is not demonstrated in any literature, except in [18].

A reverse transition would result in uncontrolled regeneration in the conventional winding changeover methods due to loss of control during the changeover. At the instant of reverse transition, the induced EMF due to permanent magnets of high equivalent turns winding will be much higher than the maximum voltage capability of the inverter. There will be a short interval during the transition when the high equivalent turns winding is connected to the inverter, and the negative d-axis current is not sufficiently high to maintain the FW. The uncontrolled regeneration would charge the dc bus capacitor to a high voltage and may also result in an overcurrent trip. Thus, it is a common practice to use the high equivalent turns only in the below base-speed region; so the terminal voltage is always within the maximum inverter limit even during the winding transition. Consequently, a significant power dip exists in the power-speed characteristics of all conventional winding changeover methods. In [18], even though a reverse transition to high equivalent turns is demonstrated, explanation of how the FW is maintained without loss of control during the transition is not provided.

In the proposed uneq0-PMSM, two separate windings (LS and HS winding) are independently fed from two inverters. Hence, during the reverse transition from "low equivalent turns (HS winding)" to "high equivalent turns (LS winding) operating in FW," a controlled high negative d-axis current is injected from HS-winding. This would maintain the FW and keep the terminal voltage of LS winding within the maximum inverter voltage capability during the transition process. As a result, the proposed uneq0-PMSM achieves a lower power dip in the combined power-speed characteristics compared to the conventional winding changeover methods.

A detailed comparison of the proposed uneq0-PMSM with the conventional winding changeover methods is given in Table III. The table entries where the proposed uneq0-PMSM gives an advantage compared to any other topology is highlighted in "light gray." Also, the major drawbacks of the existing configurations is highlighted in "dark gray" for easy understanding. The major advantages of the proposed method are as follows.

1) Reduced power dip in the power-speed characteristics due to the operation of high equivalent turns winding in the FW region.
2) Fault-tolerant operation during an open-circuit fault in any of the winding sets.
3) Absence of circulating current compared to delta connected topologies.

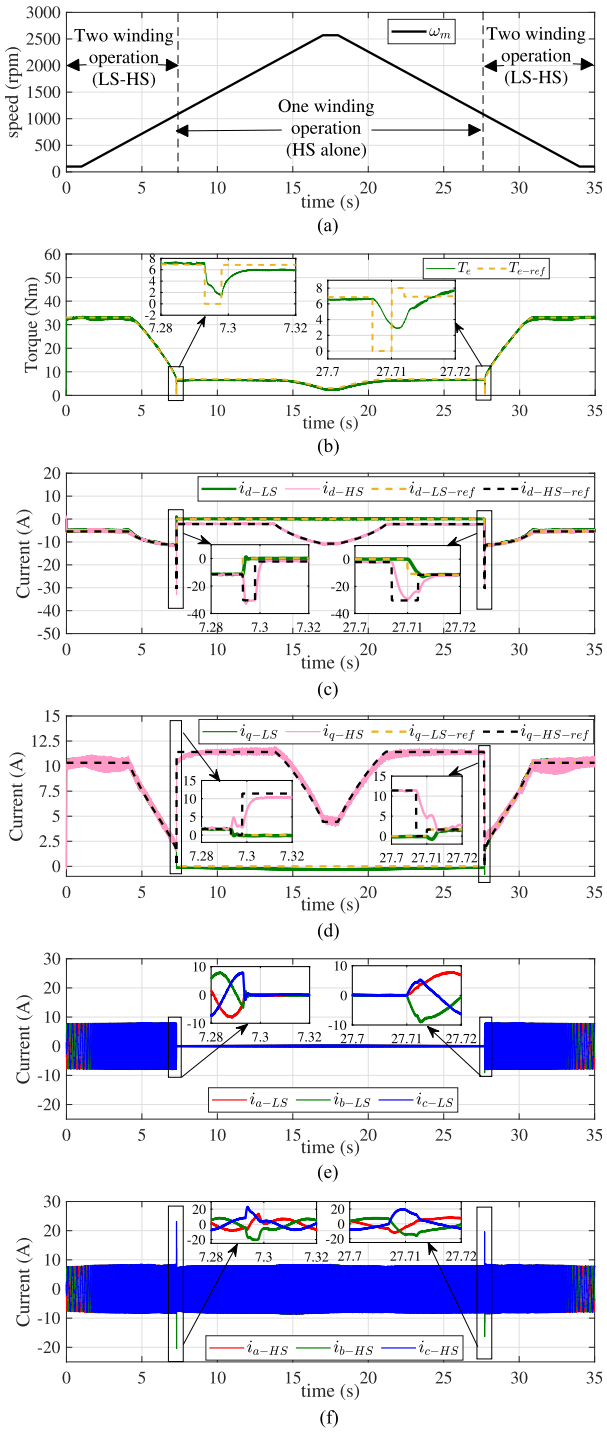

Fig. 15. Simulation results of uneq0-PMSM with proposed changeover during speed ramp-up and ramp-down. (a) Speed waveform. (b) Torque waveforms. (c) *d*-axis current waveforms. (d) *q*-axis current waveforms. (e) LS winding phase current waveform. (f) HS winding phase current waveform.

4) Improved degree of design freedom for the machine designer to choose the required torque-speed characteristics by changing the winding split ratio. Hence, the proposed method is highly suitable to achieve the high initial starting torque and wide operating speed range requirement of military vehicles and medium-/heavy-duty trucks.

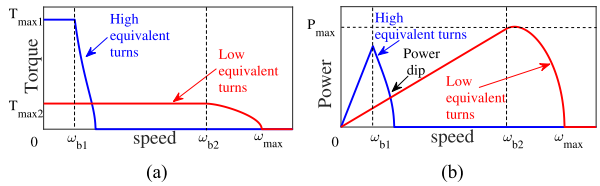

Fig. 16. General characteristics of winding changeover methods when field weakening is not used during higher equivalent number of turns operation. (a) Torque-speed. (b) Power-speed.

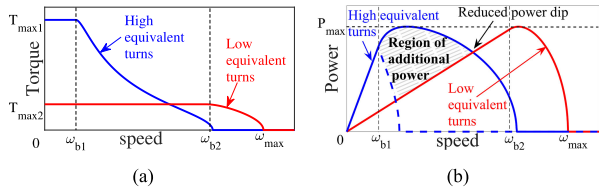

Fig. 17. General characteristics of winding changeover methods if field weakening would have been used during higher equivalent number of turns operation. (a) Torque-speed. (b) Power-speed.

5) Smooth reverse transition from "low equivalent turns" to "high equivalent turns operating in FW," without resulting in uncontrolled regeneration.

In the winding changeover methods, each bidirectional switch can be realized using two controlled switches (two IGBTs and two diodes or two thyristors). To have a one-to-one comparison of different winding topology, each IGBT is considered as one equivalent switch and each bidirectional switch is considered as two equivalent switches in all the configurations. The total number of equivalent switches in a configuration is indicative of the system cost and, hence, can be used for a cost comparison of various winding changeover configurations.

From Table III, it is observed that a lower number of equivalent switches are required in [21] (14 equivalent switches), [23] (12 equivalent switches), and [14] (eight IGBTs, two diode bridges, and four diodes) compared to 16 equivalent switches in the proposed configuration. However, none of these methods can achieve all the benefits of the proposed uneq0-PMSM, including winding open-circuit fault tolerance, reduced power dip in the combined power-speed characteristics and variable torque-speed characteristics during design.

V. Experimental Results

The proposed concept is validated on a 1.5-kW uneq0-PMSM with 1:3 split ratio with parameters given in Table IV. The machine is also reconfigured as a 2-kW DTP-PMSM by splitting the winding equally to compare the performance. The experimental setup consists of two IGBT-based two-level voltage source inverters, back-to-back thyristor switches and an induction motor coupled to the shaft of uneq0-PMSM for loading, as shown in Fig. 18. The control algorithm is implemented on Texas Instruments' TMS320F28335 digital signal processor (DSP) with 50-μs sampling time, and the switching frequency is selected as 5 kHz. The uneq0-PMSM is operated in torque control, whereas the induction motor is operated with speed control.

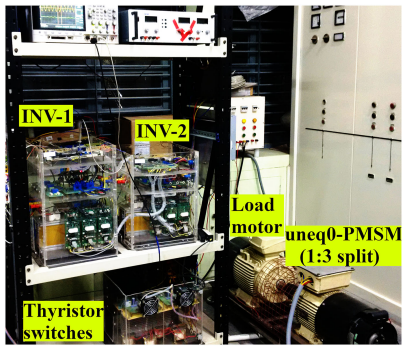

Fig. 18. Experimental setup of uneq0-PMSM fed from two inverters with back-to-back thyristor switches.

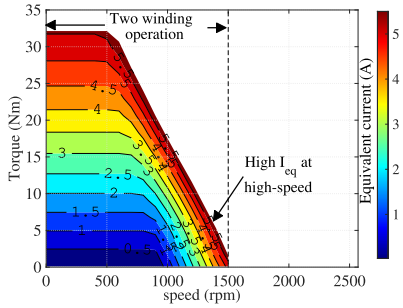

Fig. 19. Experimental results with equivalent current contours in torque-speed characteristics of DTP-PMSM.

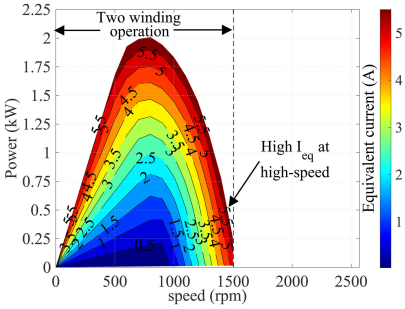

Fig. 20. Experimental results with equivalent current contours in power-speed characteristics of DTP-PMSM.

In this article, an equivalent current (I_{eq}) is defined to represent the contribution of current flowing through active conductors out of the total conductors in the machine. I_{eq} is given in terms of phase current rms ($I_{\text{ph-rms}}$) as

$$I_{\text{eq}} = I_{\text{ph-rms}} \times \frac{\text{Conducting turns per phase}}{\text{Total turns per phase}}. \tag{8}$$

Hence, for the DTP-PMSM and uneq0-PMSM during two-winding operation, I_{eq} is equal to $I_{\text{ph-rms}}$. Whereas, when HS winding is operated alone in uneq0-PMSM with 1:3 split ratio, $I_{\text{eq}}=\frac{1}{4}I_{\text{ph-rms}}$.

Figs. 19 and 20 show the equivalent current contours plotted in the torque-speed and power-speed characteristics of the DTP-PMSM. The machine has a rated torque of $32\,\text{Nm}$, $2\,\text{kW}$ at $800\,\text{r/min}$ and a maximum operating speed of $1500\,\text{r/min}$. It is observed that a higher current is necessary to operate during HS operation (beyond $800\,\text{r/min}$) compared to LS operation to

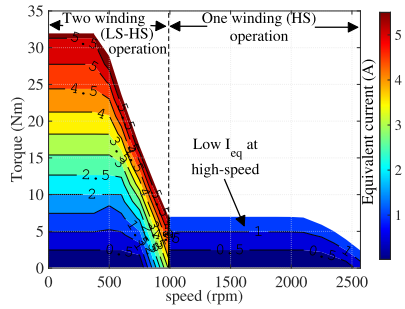

Fig. 21. Experimental results with equivalent current contours in torque-speed characteristics of the proposed uneq0-PMSM.

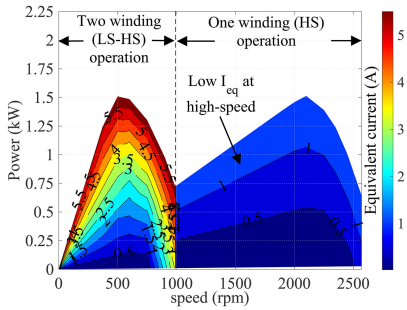

Fig. 22. Experimental results with equivalent current contours in power-speed characteristics of the proposed uneq0-PMSM.

achieve the same generated torque. This higher current demand is due to the additional d-axis current demanded to maintain the voltage within inverter limits by FW. The torque-speed and power-speed characteristics when the same three-phase PMSM is reconfigured as an uneq0-PMSM with 1:3 split ratio is shown in Figs. 21 and 22. Here, the torque-speed and power-speed characteristics have different shapes than conventional three-phase or DTP-PMSM as explained in Section III-A. Even though the initial torque-speed region appears similar to DTP-PMSM, the operating region is further extended by changing the winding configuration to HS winding alone. The one-winding operation is characterized by a wide below base-speed operation with constant torque followed by a short FW region, as observed in Fig. 21. Thus, the resulting power-speed characteristic has two peak power regions during LS and HS compared to single peak power in conventional three-phase or DTP-PMSM. It is to be noted that the peak power rating of uneq0-PMSM has reduced to $1.5\,\text{kW}$ compared to $2\,\text{kW}$ in DTP-PMSM. However, the uneq0-PMSM achieves an extended operating range up to $2570\,\text{r/min}$ compared to $1500\,\text{r/min}$ for DTP-PMSM. Further, in uneq0-PMSM, since the operation with HS winding alone does not necessitate FW for a wide speed range, the equivalent current in uneq0-PMSM is highly reduced compared to DTP-PMSM in HS operation as seen from Figs. 21 and 22.

Figs. 23 and 24 show variation of estimated generated torque ($\widehat{\text{T}}_e$), motor speed (ω_m), and phase currents of DTP-PMSM and 1:3 split uneq0-PMSM, respectively. In both machines, equal currents are injected in the two windings to achieve maximum generated torque. For DTP-PMSM, the generated torque decreases as the motor speed increases beyond base

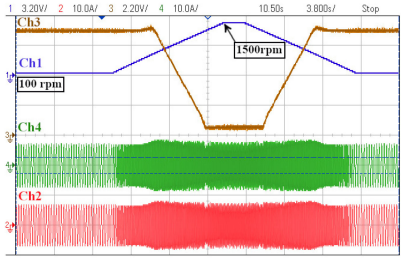

Fig. 23. Performance of DTP-PMSM during speed increase and decrease at near full load: Ch1: ω_m; Ch2: i_{a1}; Ch3: $\widehat{T}_e$; Ch4: i_{a2} (*X*-axis: 3.8 s/div; *Y*-axis: Ch1: 960 rpm/div; Ch2, Ch4: 10 A/div; Ch3: 7.49 Nm/div).

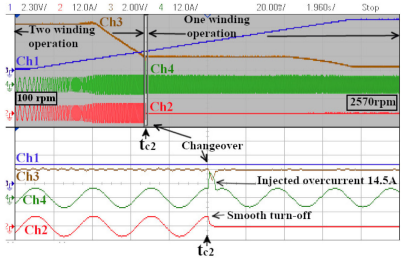

Fig. 24. Performance of uneq0-PMSM during speed increase at near full load with winding changeover: Ch1: ω_m; Ch2: $i_{a\text{-LS}}$; Ch3: $\widehat{T}_e$; Ch4: $i_{a\text{-HS}}$ (*X*-axis: 1.96 s/div; Zoom *X*-axis: 20 ms/div; *Y*-axis: Ch1: 690 r/min/div; Ch2,Ch4: 12 A/div; Ch3: 6.81 Nm/div).

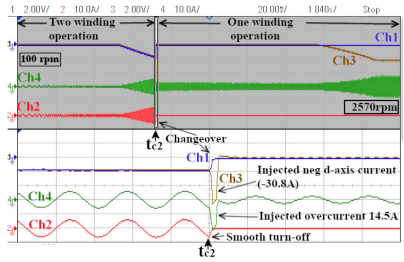

Fig. 25. Performance of uneq0-PMSM during speed increase at 2.27 Nm load with winding changeover: Ch1: $i_{d\text{-LS}}$; Ch2: $i_{a\text{-LS}}$; Ch3: $i_{d\text{-HS}}$; Ch4: $i_{a\text{-HS}}$ (*X*-axis: 1.84 s/div; Zoom *X*-axis: 20 ms/div; *Y*-axis: Ch1,Ch3: 10.18 A/div; Ch2,Ch4: 10 A/div).

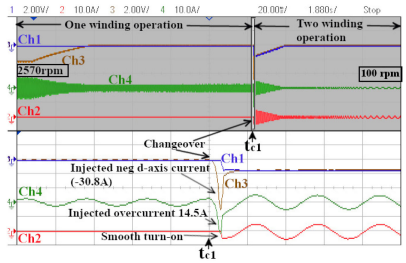

Fig. 26. Performance of uneq0-PMSM during speed decrease at 2.27 Nm load with winding changeover: Ch1: $i_{d\text{-LS}}$; Ch2: $i_{a\text{-LS}}$; Ch3: $i_{d\text{-HS}}$; Ch4: $i_{a\text{-HS}}$ (*X*-axis: 1.88 s/div; Zoom *X*-axis: 20 ms/div; *Y*-axis: Ch1,Ch3: 10.18 A/div; Ch2,Ch4: 10 A/div).

speed due to FW, as seen from Fig. 23. Even with rated current injected, the generated torque falls to nearly zero when the motor speed reaches 1500 r/min, limiting the DTP-PMSM operation. However, in the proposed uneq0-PMSM, the operating speed range is extended to 2570 r/min with the winding changeover. The generated torque decreases with speed after base speed during the two-winding operation of uneq0-PMSM, similar to DTP-PMSM. However, after 990 r/min, the generated torque is maintained constant till the base speed of HS winding by disconnecting LS winding from inverter-1 and operating HS winding alone. Thus, the extension of torque-speed characteristics and wide below base-speed operating region of uneq0-PMSM is demonstrated experimentally. The smooth transition from two-winding operation to one-winding in Fig. 24 is achieved by injecting a high negative d-axis current (30.8 A) in HS winding for a short duration (5 ms) as explained in Section III-C. The d-axis current in HS winding for a smooth transition is calculated as 4×7.7 A, where 7.7 A corresponds to the minimum value required to maintain FW with zero generated torque while both windings were operating together. The additional d-axis current is reflected in the phase current (14.5 A-rms) as observed from the zoomed waveforms in Fig. 24. The additional d-axis current increases with a higher difference in the winding turns between LS and HS winding. Hence, the switches and thermal rating of the inverter should be designed to deliver this additional current in HS winding for a short duration during the winding transition. It should be noted that, for heavy-duty transport trucks and military vehicles, the inverter would necessarily have a high short-time rating for satisfying the intermittent load requirements as discussed in Section II.

Variation of d-axis current of LS and HS winding during speed increase and decrease at a constant load of 2.27 Nm is shown in Figs. 25 and 26. From Fig. 25, it is observed that d-axis current increases in both LS and HS winding as the machine speed increases beyond the base speed of combined LS-HS winding operation due to FW. However, once the operation changes to one-winding at 990 r/min, the d-axis current demand decreases drastically since the machine with only HS winding active operates in the below base-speed region. The winding currents of LS winding become zero after it is disconnected from inverter-1 using the thyristor switches, as seen in Fig. 25. As the machine speed increases further, FW is initiated in HS winding by injecting a higher d-axis current to reach the final speed of 2570 r/min. Injection of additional negative d-axis current in HS winding during the winding changeover is observed in the zoomed waveforms of Figs. 25 and 26. Thus, a seamless transition from two-winding to one-winding and vice versa with controlled currents is achieved in the proposed uneq0-PMSM.

Steady-state operation of uneq0-PMSM at 990 r/min at full load is shown in Fig. 27. The modulation index of LS winding is nearly three times the HS winding since the winding split ratio of uneq0-PMSM is 1:3. Also, the phase currents of LS and HS winding are equal in magnitude and phase and are nice sinusoids without any significant lower order harmonics.

VI. Conclusion

In this article, an unequal split DTP-PMSM with 0° winding displacement (uneq0-PMSM) operated with two inverters with a common dc bus and two back-to-back thyristor switches is proposed for improved performance of medium-/heavy-duty

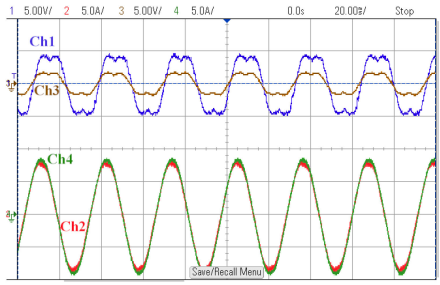

Fig. 27. Steady-state operation of uneq0-PMSM at 990 r/min under full load: Ch1: $m_{a\text{-LS}}$; Ch2: $i_{a\text{-LS}}$; Ch3: $m_{a\text{-HS}}$; Ch4: $i_{a\text{-HS}}$ (*X*-axis:- 20 ms/div; *Y*-axis:- Ch1,Ch3: 1 p u./div; Ch2,Ch4: 5 A/div).

trucks and military vehicles. The uneq0-PMSM has a better overload capability than high CPSR three-phase PMSM and reduced power rating than low CPSR three-phase PMSM for satisfying the same load requirement. Further, the shape of torque-speed characteristics of uneq0-PMSM can be modified by varying the winding split ratio to suit the application. The wide speed range of uneq0-PMSM with below base-speed operation in most operating points also reduces the additional d-axis current requirement compared to FW in conventional three-phase PMSM. Finally, a transition algorithm for smooth winding changeover between two-winding operation (combined LS-HS winding) and one-winding operation (HS winding alone) is also proposed. The proposed concepts are experimentally validated on a 1.5-kW uneq0-PMSM with 1:3 split ratio.

APPENDIX A
DYNAMIC MODELING OF UNEQ0-PMSM

For all the parameters, subscript "LS" denotes that it belongs to LS winding, "HS" denotes that it belongs to HS winding, and "LSHS" denotes the mutual terms. Assume that uneq0-PMSM has a winding split ratio of n_{HS}:n_{LS}, where n_{LS} and n_{HS} represent the number of turns per phase of LS winding and HS winding, respectively. The parameters of uneq0-PMSM can be represented in terms of three-phase PMSM parameters as $R_{s\text{-LS}}{=}d_1R_s$; $L_{ls\text{-LS}}{=}d_1^2L_{ls}$; $\Psi_{F\text{-LS}}{=}d_1\Psi_F$; $L_{md\text{-LS}}{=}d_1^2L_{md}$; $L_{mq\text{-LS}}{=}d_1^2L_{mq}$; $R_{s\text{-HS}}{=}d_2R_s$; $L_{ls\text{-HS}}{=}d_2^2L_{ls}$; $\Psi_{F\text{-HS}}{=}d_2\Psi_F$; $L_{md\text{-HS}}{=}d_2^2L_{md}$; $L_{mq\text{-HS}}{=}d_2^2L_{mq}$; $L_{md\text{-LSHS}}{=}d_1d_2L_{md}$; $L_{mq\text{-LSHS}}{=}d_1d_2L_{mq}$ where R_s is the per phase stator resistance, Ψ_F is the permanent magnet flux, L_{md} is the d-axis magnetizing inductance, L_{mq} is the q-axis magnetizing inductance, and L_{ls} is the self-leakage inductance of the original three-phase PMSM from which the uneq0-PMSM was derived. Here, $d_1{=}\frac{n_{\text{LS}}}{n_{\text{LS}}+n_{\text{HS}}}$; $d_2{=}\frac{n_{\text{HS}}}{n_{\text{LS}}+n_{\text{HS}}}$.

The stator voltage equations of uneq0-PMSM in synchronous $d-q$ frame are given by

$$\begin{aligned} v_{d\text{-LS}} &= R_{s\text{-LS}}i_{d\text{-LS}} + (L_{ls\text{-LS}}{+}L_{md\text{-LS}})\frac{d}{dt}i_{d\text{-LS}} \\ &\quad + (L'_{lm}{+}L_{md\text{-LSHS}})\frac{d}{dt}i_{d\text{-HS}}{-}\omega_e(L_{ls\text{-LS}}{+}L_{mq\text{-LS}})i_{q\text{-LS}} \\ &\quad -\omega_e(L'_{lm}{+}L_{mq\text{-LSHS}})i_{q\text{-HS}} \end{aligned} \tag{9}$$

$$\begin{aligned} v_{q\text{-LS}} &= R_{s\text{-LS}}i_{q\text{-LS}} + (L_{ls\text{-LS}}{+}L_{mq\text{-LS}})\frac{d}{dt}i_{q\text{-LS}} \\ &\quad + (L'_{lm}{+}L_{mq\text{-LSHS}})\frac{d}{dt}i_{q\text{-HS}}{+}\omega_e(L_{ls\text{-LS}}{+}L_{md\text{-LS}})i_{d\text{-LS}} \\ &\quad +\omega_e(L'_{lm}{+}L_{md\text{-LSHS}})i_{d\text{-HS}} + \frac{3}{2}\omega_e\Psi_{F\text{-LS}} \end{aligned} \tag{10}$$

$$\begin{aligned} v_{d\text{-HS}} &= R_{s\text{-HS}}i_{d\text{-HS}} + (L_{ls\text{-HS}}{+}L_{md\text{-HS}})\frac{d}{dt}i_{d\text{-HS}} \\ &\quad +(L'_{lm}{+}L_{md\text{-LSHS}})\frac{d}{dt}i_{d\text{-LS}}{-}\omega_e(L_{ls\text{-HS}}{+}L_{mq\text{-HS}})i_{q\text{-HS}} \\ &\quad -\omega_e(L'_{lm}{+}L_{mq\text{-LSHS}})i_{q\text{-LS}} \end{aligned} \tag{11}$$

$$\begin{aligned} v_{q\text{-HS}} &= R_{s\text{-HS}}i_{q\text{-HS}} + (L_{ls\text{-HS}}{+}L_{mq\text{-HS}})\frac{d}{dt}i_{q\text{-HS}} \\ &\quad +(L'_{lm}{+}L_{mq\text{-LSHS}})\frac{d}{dt}i_{q\text{-LS}}{+}\omega_e(L_{ls\text{-HS}}{+}L_{md\text{-HS}})i_{d\text{-HS}} \\ &\quad +\omega_e(L'_{lm}{+}L_{md\text{-LSHS}})i_{d\text{-LS}} + \frac{3}{2}\omega_e\Psi_{F\text{-HS}} \end{aligned} \tag{12}$$

where ω_e is the electrical rotor speed, $L_{md\text{-LSHS}}$ is the mutual inductance between LS and HS winding, and L'_{lm} is the mutual leakage inductance between LS and HS winding.

REFERENCES

[1] A. S. Mohammadi, J. P. Trovão, and M. R. Dubois, "Hybridisation ratio for hybrid excitation synchronous motors in electric vehicles with enhanced performance," *IET Elect. Syst. Transp.*, vol. 8, no. 7, pp. 12–19, Mar. 2018. [Online]. Available: https://digital-library.theiet.org/content/journals/10.1049/iet-est.2017.0029

[2] F. Giulii Capponi, G. Borocci, G. De Donato, and F. Caricchi, "Flux regulation strategies for hybrid excitation synchronous machines," *IEEE Trans. Ind. Appl.*, vol. 51, no. 5, pp. 3838–3847, Sep./Oct. 2015.

[3] W. Soong and N. Ertugrul, "Field-weakening performance of interior permanent-magnet motors," *IEEE Trans. Ind. Appl.*, vol. 38, no. 5, pp. 1251–1258, Sep./Oct. 2002.

[4] P. Chapman and P. Krein, "Motor re-rating for traction applications - field weakening revisited," in *Proc. IEEE Int. Electric Mach. Drives Conf.*, 2003, pp. 1388–1391.

[5] A. Amerise, L. Rovere, A. Formentini, M. Mengoni, L. Zarri, and P. Zanchetta, "Electric drive based on an open-end winding surface PM synchronous machine with a floating capacitor bridge," *IEEE Trans. Ind. Appl.*, vol. 56, no. 3, pp. 2709–2718, May/Jun. 2020.

[6] D. Pan, F. Liang, Y. Wang, and T. A. Lipo, "Extension of the operating region of an IPM motor utilizing series compensation," *IEEE Trans. Ind. Appl.*, vol. 50, no. 1, pp. 539–548, Jan./Feb. 2014.

[7] S. V. Nair, H. K. P., and K. Hatua, "Six-step operation of a symmetric dual three-phase PMSM with minimal circulating currents for extended speed range in electric vehicles," *IEEE Trans. Ind. Electron.*, vol. 69, no. 8, pp. 7651–7662, Aug. 2022.

[8] S. Atiq, T. A. Lipo, and B.-I. Kwon, "Wide speed range operation of non-salient PM machines," *IEEE Trans. Energy Convers.*, vol. 31, no. 3, pp. 1179–1191, Sep. 2016.

[9] S. Zhitkova and K. Hameyer, "Realization of a wide speed range for an agricultural tractor," in *Proc. 22th Int. Conf. Elect. Mach.*, 2016, pp. 2031–2037.

[10] C.-H. Chen and M.-Y. Cheng, "Design of a multispeed winding for a brushless DC motor and its sensorless control," *IEE Proc. - Electric Power Appl.*, vol. 153, pp. 834–841, Nov. 2006. [Online]. Available: https://digital-library.theiet.org/content/journals/10.1049/ip-epa_20060073

[11] T. Kume, T. Iwakane, T. Sawa, T. Yoshida, and I. Nagai, "A wide constant power range vector-controlled AC motor drive using winding changeover technique," *IEEE Trans. Ind. Appl.*, vol. 27, no. 5, pp. 934–939, Sep./Oct. 1991.

[12] H. Hijikata and K. Akatsu, "Design and online winding reconfigurations method of matrix motor," in *Proc. IEEE Energy Convers. Congr. Expo.*, 2012, pp. 1330–1337.
[13] H. Hijikata, Y. Sakai, K. Akatsu, Y. Miyama, H. Arita, and A. Daikoku, "Wide speed range operation by low-voltage inverter-fed matrix motor for automobile traction motor," *IEEE Trans. Power Electron.*, vol. 33, no. 8, pp. 6887–6896, Aug. 2018.
[14] M. Swamy, T. Kume, A. Maemura, and S. Morimoto, "Extended high-speed operation via electronic winding-change method for AC motors," *IEEE Trans. Ind. Appl.*, vol. 42, no. 3, pp. 742–752, May/Jun. 2006.
[15] Y. Gao, H. Maghbelli, M. Ehsani, G. Frazier, J. Kajs, and S. Bayne, "Investigation of proper motor drive characteristics for military vehicle propulsion," in *Proc. Future Transp. Technol. Conf. Expo.*, 2003, pp. 1–7. [Online]. Available: https://doi.org/10.4271/2003-01-2296
[16] W. Soong and T. Miller, "Theoretical limitations to the field-weakening performance of the five classes of brushless synchronous AC motor drive," in *Proc. 6th Int. Conf. Elect. Mach. Drives*, 1993, pp. 127–132.
[17] K. Hatua and S. V. Nair, "Programmable torque-speed characteristics drive for extended constant power region and high efficiency in PMSM and BLDC drives," Indian Patent 201 941 028 573, Jul. 16, 2019.
[18] S. Atiq, T. A. Lipo, and B.-i. Kwon, "Experimental verification of winding switching technique to enhance maximum speed operation of surface mounted permanent magnet machines," *IET Electric Power Appl.*, vol. 10, no. 4, pp. 294–303, 2016.
[19] T. Kume, T. Sawa, M. Miyazato, M. Sawamura, and M. Zenke, "Inverter driving method for induction motors," U.S. Patent 4 916 376, Apr. 10, 1990.
[20] M.-S. Wang, N.-C. Hsu, C.-Y. Chiang, S.-H. Wang, and T.-C. Shau, "A novel changeover technique for variable-winding brushless DC motor drives," in *Proc. SICE Annu. Conf.* 2010, pp. 2650–2653.
[21] T. Kume and T. Sawa, "A static winding changeover technique," Japanese Patent 799 959, Oct. 25, 1995.
[22] H. Huang and L. Chang, "Electrical two-speed propulsion by motor winding switching and its control strategies for electric vehicles," *IEEE Trans. Veh. Technol.*, vol. 48, no. 2, pp. 607–618, Mar. 1999.
[23] S.-H. Im and B.-G. Gu, "A snubberless solid-state tap changer for permanent magnet synchronous motors," *IEEE Trans. Power Electron.*, vol. 35, no. 11, pp. 12143–12152, Nov. 2020.
[24] M.-F. Hsieh, F.-S. Hsu, and D. G. Dorrell, "Winding changeover permanent-magnet generators for renewable energy applications," *IEEE Trans. Magn.*, vol. 48, no. 11, pp. 4168–4171, Nov. 2012.
[25] S. Sadeghi, L. Guo, H. A. Toliyat, and L. Parsa, "Wide operational speed range of five-phase permanent magnet machines by using different stator winding configurations," *IEEE Trans. Ind. Electron.*, vol. 59, no. 6, pp. 2621–2631, Jun. 2012.
[26] A. Li, D. Jiang, X. Sun, and Z. Liu, "Online drive topology conversion technology for PMSM speed range extension," *IEEE Trans. Power Electron.*, vol. 37, no. 6, pp. 7113–7121, Jun. 2022.
[27] S. Sin, M. Ayub, and B.-I. Kwon, "Operation method of non-salient permanent magnet synchronous machine for extended speed range," *IEEE Access*, vol. 8, pp. 105922–105935, 2020.
[28] S. Sin, M. Ayub, and B.-I. Kwon, "Investigation study of multi-mode multi-speed operation method for surface-mounted permanent magnet synchronous machines," *IEEE Access*, vol. 8, pp. 169470–169485, 2020.

Sandeep V. Nair (Student Member, IEEE) was born in Kerala, India. He received the B.Tech. degree in electrical and electronics engineering from the NSS College of Engineering (affiliated to Calicut University), Palakkad, India, in 2011, and the M.Tech. degree in electrical engineering from the Indian Institute of Technology Bombay, Mumbai, India, in 2015. He is currently working toward the Ph.D. degree in electrical engineering with the Indian Institute of Technology Madras, Chennai, India.

His research interests include design of electric machines, starting methods for permanent magnet synchronous motor drives, multiphase machines, and real-time simulation of power electronics and power systems.

Kunal Layek was born in Durgapur, West Bengal, India. He received the B.Tech. degree in electrical engineering from Asansol Engineering College, Asansol, India, in 2013. He is currently working toward the integrated M.S. and Ph.D. degree in electrical engineering with the Indian Institute of Technology Madras, Chennai, India.

He joined L&T Construction, Power Transmission and Distribution IC, in 2013 and worked for six years. His research interests include PMSM and SynRM drives for EV applications.

Kamalesh Hatua (Member, IEEE) was born in West Bengal, India. He received the B.E. degree in electrical and electronics engineering from Karnataka Regional Engineering College, Surathkal, India, in 2000, and the M.Sc. and Ph.D. degrees in electrical engineering from the Indian Institute of Science Bangalore, Bangalore, India, in 2004 and 2011, respectively.

He was with Bharat Earth Movers Ltd., Mysore, India, for the development of computerized transmission controller for dumpers. He was also with the Honeywell Technology Solutions Laboratory, Bangalore, for the development of the inverter for aerospace applications. He was a Postdoctoral Research Fellow with the Future Renewable Electrical Energy Delivery and Management (FREEDM) Center, North Carolina State University, Raleigh, NC, USA, for the development of the SiC device based solid-state transformer from 2010 to 2012. He is currently an Associate Professor with the Department of Electrical Engineering, Indian Institute of Technology Madras, Chennai, India. His research interests include medium-voltage electric drives, automotive drives, polyphase induction motor drives, active gate driving for SiC switches, solid-state transformer, power electronics application in power system, and design of highly efficient power converters using SiC power switches.